

J/ψ Production vs Transverse Momentum and Rapidity
in *p+p* Collisions at $\sqrt{s} = 200$ GeV

A. Adare,⁸ S. Afanasiev,²² C. Aidala,⁹ N.N. Ajitanand,⁴⁸ Y. Akiba,^{42,43} H. Al-Bataineh,³⁷ J. Alexander,⁴⁸ K. Aoki,^{27,42} L. Aphecetche,⁵⁰ R. Armendariz,³⁷ S.H. Aronson,³ J. Asai,⁴³ E.T. Atomssa,²⁸ R. Averbeck,⁴⁹ T.C. Awes,³⁸ B. Azmoun,³ V. Babintsev,¹⁸ G. Baksay,¹⁴ L. Baksay,¹⁴ A. Baldisseri,¹¹ K.N. Barish,⁴ P.D. Barnes,³⁰ B. Bassalleck,³⁶ S. Bathe,⁴ S. Batsouli,³⁸ V. Baublis,⁴¹ A. Bazilevsky,³ S. Belikov,³ R. Bennett,⁴⁹ Y. Berdnikov,⁴⁵ A.A. Bickley,⁸ J.G. Boissevain,³⁰ H. Borel,¹¹ K. Boyle,⁴⁹ M.L. Brooks,³⁰ H. Buesching,³ V. Bumazhnov,¹⁸ G. Bunce,^{3,43} S. Butsyk,^{30,49} S. Campbell,⁴⁹ B.S. Chang,⁵⁷ J.-L. Charvet,¹¹ S. Chernichenko,¹⁸ J. Chiba,²³ C.Y. Chi,⁹ M. Chiu,¹⁹ I.J. Choi,⁵⁷ T. Chujo,⁵⁴ P. Chung,⁴⁸ A. Churym,¹⁸ V. Cianciolo,³⁸ C.R. Cleven,¹⁶ B.A. Cole,⁹ M.P. Comets,³⁹ P. Constantin,³⁰ M. Csanád,¹³ T. Csörgő,²⁴ T. Dahms,⁴⁹ K. Das,¹⁵ G. David,³ M.B. Deaton,¹ K. Dehmelt,¹⁴ H. Delagrangé,⁵⁰ A. Denisov,¹⁸ D. d'Enterria,⁹ A. Deshpande,^{43,49} E.J. Desmond,³ O. Dietzsch,⁴⁶ A. Dion,⁴⁹ M. Donadelli,⁴⁶ O. Drapier,²⁸ A. Drees,⁴⁹ A.K. Dubey,⁵⁶ A. Durum,¹⁸ V. Dzhordzhadze,⁴ Y.V. Efremenko,³⁸ J. Egdemir,⁴⁹ F. Ellinghaus,⁸ W.S. Emam,⁴ A. Enokizono,²⁹ H. En'yo,^{42,43} S. Esumi,⁵³ K.O. Eyser,⁴ D.E. Fields,^{36,43} M. Finger,^{5,22} M. Finger, Jr.,^{5,22} F. Fleuret,²⁸ S.L. Fokin,²⁶ Z. Fraenkel,⁵⁶ J.E. Frantz,⁴⁹ A. Franz,³ A.D. Frawley,¹⁵ K. Fujiwara,⁴² Y. Fukao,^{27,42} T. Fusayasu,³⁵ S. Gadrat,³¹ I. Garishvili,⁵¹ A. Glenn,⁸ H. Gong,⁴⁹ M. Gonin,²⁸ J. Gosset,¹¹ Y. Goto,^{42,43} R. Granier de Cassagnac,²⁸ N. Grau,²¹ S.V. Greene,⁵⁴ M. Grosse Perdekamp,^{19,43} T. Gunji,⁷ H.-Å. Gustafsson,³² T. Hachiya,¹⁷ A. Hadj Henni,⁵⁰ C. Haegemann,³⁶ J.S. Haggerty,³ H. Hamagaki,⁷ R. Han,⁴⁰ H. Harada,¹⁷ E.P. Hartouni,²⁹ K. Haruna,¹⁷ E. Haslum,³² R. Hayano,⁷ M. Heffner,²⁹ T.K. Hemmick,⁴⁹ T. Hester,⁴ X. He,¹⁶ H. Hiejima,¹⁹ J.C. Hill,²¹ R. Hobbs,³⁶ M. Hohlmann,¹⁴ W. Holzmann,⁴⁸ K. Homma,¹⁷ B. Hong,²⁵ T. Horaguchi,^{42,52} D. Hornback,⁵¹ T. Ichihara,^{42,43} K. Imai,^{27,42} M. Inaba,⁵³ Y. Inoue,^{44,42} D. Isenhowe,¹ L. Isenhowe,¹ M. Ishihara,⁴² T. Isobe,⁷ M. Issah,⁴⁸ A. Isupov,²² B.V. Jacak,⁴⁹ J. Jia,⁹ J. Jin,⁹ O. Jinnouchi,⁴³ B.M. Johnson,³ K.S. Joo,³⁴ D. Jouan,³⁹ F. Kajihara,⁷ S. Kametani,^{7,55} N. Kamihara,⁴² J. Kamin,⁴⁹ M. Kaneta,⁴³ J.H. Kang,⁵⁷ H. Kanou,^{42,52} D. Kawall,⁴³ A.V. Kazantsev,²⁶ A. Khanzadeev,⁴¹ J. Kikuchi,⁵⁵ D.H. Kim,³⁴ D.J. Kim,⁵⁷ E. Kim,⁴⁷ E. Kinney,⁸ A. Kiss,¹³ E. Kistenev,³ A. Kiyomichi,⁴² J. Klay,²⁹ C. Klein-Boesing,³³ L. Kochenda,⁴¹ V. Kochetkov,¹⁸ B. Komkov,⁴¹ M. Konno,⁵³ D. Kotchetkov,⁴ A. Kozlov,⁵⁶ A. Král,¹⁰ A. Kravitz,⁹ J. Kubart,^{5,20} G.J. Kunde,³⁰ N. Kurihara,⁷ K. Kurita,^{44,42} M.J. Kweon,²⁵ Y. Kwon,^{51,57} G.S. Kyle,³⁷ R. Lacey,⁴⁸ Y.-S. Lai,⁹ J.G. Lajoie,²¹ A. Lebedev,²¹ D.M. Lee,³⁰ M.K. Lee,⁵⁷ T. Lee,⁴⁷ M.J. Leitch,³⁰ M.A.L. Leite,⁴⁶ B. Lenzi,⁴⁶ T. Liška,¹⁰ A. Litvinenko,²² M.X. Liu,³⁰ X. Li,⁶ B. Love,⁵⁴ D. Lynch,³ C.F. Maguire,⁵⁴ Y.I. Makdisi,³ A. Malakhov,²² M.D. Malik,³⁶ V.I. Manko,²⁶ Y. Mao,^{40,42} L. Mašek,^{5,20} H. Masui,⁵³ F. Matathias,⁹ M. McCumber,⁴⁹ P.L. McGaughey,³⁰ Y. Miake,⁵³ P. Mikeš,^{5,20} K. Miki,⁵³ T.E. Miller,⁵⁴ A. Milov,⁴⁹ S. Mioduszewski,³ M. Mishra,² J.T. Mitchell,³ M. Mitrovski,⁴⁸ A. Morreale,⁴ D.P. Morrison,³ T.V. Moukhanova,²⁶ D. Mukhopadhyay,⁵⁴ J. Murata,^{44,42} S. Nagamiya,²³ Y. Nagata,⁵³ J.L. Nagle,⁸ M. Naglis,⁵⁶ I. Nakagawa,^{42,43} Y. Nakamiya,¹⁷ T. Nakamura,¹⁷ K. Nakano,^{42,52} J. Newby,²⁹ M. Nguyen,⁴⁹ B.E. Norman,³⁰ A.S. Nyanin,²⁶ E. O'Brien,³ S.X. Oda,⁷ C.A. Ogilvie,²¹ H. Ohnishi,⁴² H. Okada,^{27,42} K. Okada,⁴³ M. Oka,⁵³ O.O. Omiwade,¹ A. Oskarsson,³² M. Ouchida,¹⁷ K. Ozawa,⁷ R. Pak,³ D. Pal,⁵⁴ A.P.T. Palounek,³⁰ V. Pantuev,⁴⁹ V. Papavassiliou,³⁷ J. Park,⁴⁷ W.J. Park,²⁵ S.F. Pate,³⁷ H. Pei,²¹ J.-C. Peng,¹⁹ H. Pereira,¹¹ V. Peresedov,²² D.Yu. Peressounko,²⁶ C. Pinkenburg,³ M.L. Purschke,³ A.K. Purwar,³⁰ H. Qu,¹⁶ J. Rak,³⁶ A. Rakotozafindrabe,²⁸ I. Ravinovich,⁵⁶ K.F. Read,^{38,51} S. Rembeczki,¹⁴ M. Reuter,⁴⁹ K. Reygers,³³ V. Riabov,⁴¹ Y. Riabov,⁴¹ G. Roche,³¹ A. Romana,^{28,*} M. Rosati,²¹ S.S.E. Rosendahl,³² P. Rosnet,³¹ P. Rukoyatkin,²² V.L. Rykov,⁴² B. Sahlmueller,³³ N. Saito,^{27,42,43} T. Sakaguchi,³ S. Sakai,⁵³ H. Sakata,¹⁷ V. Samsonov,⁴¹ S. Sato,²³ S. Sawada,²³ J. Seele,⁸ R. Seidl,¹⁹ V. Semenov,¹⁸ R. Seto,⁴ D. Sharma,⁵⁶ I. Shein,¹⁸ A. Shevel,^{41,48} T.-A. Shibata,^{42,52} K. Shigaki,¹⁷ M. Shimomura,⁵³ K. Shoji,^{27,42} A. Sickles,⁴⁹ C.L. Silva,⁴⁶ D. Silvermyr,³⁸ C. Silvestre,¹¹ K.S. Sim,²⁵ C.P. Singh,² V. Singh,² S. Skutnik,²¹ M. Slunečka,^{5,22} A. Soldatov,¹⁸ R.A. Soltz,²⁹ W.E. Sondheim,³⁰ S.P. Sorensen,⁵¹ I.V. Sourikova,³ F. Staley,¹¹ P.W. Stankus,³⁸ E. Stenlund,³² M. Stepanov,³⁷ A. Ster,²⁴ S.P. Stoll,³ T. Sugitate,¹⁷ C. Suire,³⁹ J. Sziklai,²⁴ T. Tabaru,⁴³ S. Takagi,⁵³ E.M. Takagui,⁴⁶ A. Taketani,^{42,43} Y. Tanaka,³⁵ K. Tanida,^{42,43} M.J. Tannenbaum,³ A. Taranenko,⁴⁸ P. Tarján,¹² T.L. Thomas,³⁶ M. Togawa,^{27,42} A. Toia,⁴⁹ J. Tojo,⁴² L. Tomášek,²⁰ H. Torii,⁴² R.S. Towell,¹ V.-N. Tram,²⁸ I. Tserruya,⁵⁶ Y. Tsuchimoto,¹⁷ C. Vale,²¹ H. Valle,⁵⁴ H.W. van Hecke,³⁰ J. Velkovska,⁵⁴ R. Vertesi,¹² A.A. Vinogradov,²⁶ M. Virius,¹⁰ V. Vrba,²⁰ E. Vznuzdaev,⁴¹ M. Wagner,^{27,42} D. Walker,⁴⁹ X.R. Wang,³⁷ Y. Watanabe,^{42,43} J. Wessels,³³ S.N. White,³ D. Winter,⁹ C.L. Woody,³ M. Wysocki,⁸

W. Xie,⁴³ Y. Yamaguchi,⁵⁵ A. Yanovich,¹⁸ Z. Yasin,⁴ J. Ying,¹⁶ S. Yokkaichi,^{42,43} G.R. Young,³⁸ I. Younus,³⁶
 I.E. Yushmanov,²⁶ W.A. Zajc,^{9,†} O. Zaudtke,³³ C. Zhang,³⁸ S. Zhou,⁶ J. Zimányi,^{24,*} and L. Zolin²²
 (PHENIX Collaboration)

- ¹Abilene Christian University, Abilene, TX 79699, U.S.
²Department of Physics, Banaras Hindu University, Varanasi 221005, India
³Brookhaven National Laboratory, Upton, NY 11973-5000, U.S.
⁴University of California - Riverside, Riverside, CA 92521, U.S.
⁵Charles University, Ovocný trh 5, Praha 1, 116 36, Prague, Czech Republic
⁶China Institute of Atomic Energy (CIAE), Beijing, People's Republic of China
⁷Center for Nuclear Study, Graduate School of Science, University of Tokyo, 7-3-1 Hongo, Bunkyo, Tokyo 113-0033, Japan
⁸University of Colorado, Boulder, CO 80309, U.S.
⁹Columbia University, New York, NY 10027 and Nevis Laboratories, Irvington, NY 10533, U.S.
¹⁰Czech Technical University, Zikova 4, 166 36 Prague 6, Czech Republic
¹¹Dapnia, CEA Saclay, F-91191, Gif-sur-Yvette, France
¹²Debrecen University, H-4010 Debrecen, Egyetem tér 1, Hungary
¹³ELTE, Eötvös Loránd University, H - 1117 Budapest, Pázmány P. s. 1/A, Hungary
¹⁴Florida Institute of Technology, Melbourne, FL 32901, U.S.
¹⁵Florida State University, Tallahassee, FL 32306, U.S.
¹⁶Georgia State University, Atlanta, GA 30303, U.S.
¹⁷Hiroshima University, Kagamiyama, Higashi-Hiroshima 739-8526, Japan
¹⁸IHEP Protvino, State Research Center of Russian Federation, Institute for High Energy Physics, Protvino, 142281, Russia
¹⁹University of Illinois at Urbana-Champaign, Urbana, IL 61801, U.S.
²⁰Institute of Physics, Academy of Sciences of the Czech Republic, Na Slovance 2, 182 21 Prague 8, Czech Republic
²¹Iowa State University, Ames, IA 50011, U.S.
²²Joint Institute for Nuclear Research, 141980 Dubna, Moscow Region, Russia
²³KEK, High Energy Accelerator Research Organization, Tsukuba, Ibaraki 305-0801, Japan
²⁴KFKI Research Institute for Particle and Nuclear Physics of the Hungarian Academy of Sciences (MTA KFKI RMKI), H-1525 Budapest 114, POBox 49, Budapest, Hungary
²⁵Korea University, Seoul, 136-701, Korea
²⁶Russian Research Center "Kurchatov Institute", Moscow, Russia
²⁷Kyoto University, Kyoto 606-8502, Japan
²⁸Laboratoire Leprince-Ringuet, Ecole Polytechnique, CNRS-IN2P3, Route de Saclay, F-91128, Palaiseau, France
²⁹Lawrence Livermore National Laboratory, Livermore, CA 94550, U.S.
³⁰Los Alamos National Laboratory, Los Alamos, NM 87545, U.S.
³¹LPC, Université Blaise Pascal, CNRS-IN2P3, Clermont-Fd, 63177 Aubiere Cedex, France
³²Department of Physics, Lund University, Box 118, SE-221 00 Lund, Sweden
³³Institut für Kernphysik, University of Muenster, D-48149 Muenster, Germany
³⁴Myongji University, Yongin, Kyonggido 449-728, Korea
³⁵Nagasaki Institute of Applied Science, Nagasaki-shi, Nagasaki 851-0193, Japan
³⁶University of New Mexico, Albuquerque, NM 87131, U.S.
³⁷New Mexico State University, Las Cruces, NM 88003, U.S.
³⁸Oak Ridge National Laboratory, Oak Ridge, TN 37831, U.S.
³⁹IPN-Orsay, Université Paris Sud, CNRS-IN2P3, BP1, F-91406, Orsay, France
⁴⁰Peking University, Beijing, People's Republic of China
⁴¹PNPI, Petersburg Nuclear Physics Institute, Gatchina, Leningrad region, 188300, Russia
⁴²RIKEN, The Institute of Physical and Chemical Research, Wako, Saitama 351-0198, Japan
⁴³RIKEN BNL Research Center, Brookhaven National Laboratory, Upton, NY 11973-5000, U.S.
⁴⁴Physics Department, Rikkyo University, 3-34-1 Nishi-Ikebukuro, Toshima, Tokyo 171-8501, Japan
⁴⁵Saint Petersburg State Polytechnic University, St. Petersburg, Russia
⁴⁶Universidade de São Paulo, Instituto de Física, Caixa Postal 66318, São Paulo CEP05315-970, Brazil
⁴⁷System Electronics Laboratory, Seoul National University, Seoul, South Korea
⁴⁸Chemistry Department, Stony Brook University, Stony Brook, SUNY, NY 11794-3400, U.S.
⁴⁹Department of Physics and Astronomy, Stony Brook University, SUNY, Stony Brook, NY 11794, U.S.
⁵⁰SUBATECH (Ecole des Mines de Nantes, CNRS-IN2P3, Université de Nantes) BP 20722 - 44307, Nantes, France
⁵¹University of Tennessee, Knoxville, TN 37996, U.S.
⁵²Department of Physics, Tokyo Institute of Technology, Oh-okayama, Meguro, Tokyo 152-8551, Japan
⁵³Institute of Physics, University of Tsukuba, Tsukuba, Ibaraki 305, Japan
⁵⁴Vanderbilt University, Nashville, TN 37235, U.S.
⁵⁵Waseda University, Advanced Research Institute for Science and Engineering, 17 Kikui-cho, Shinjuku-ku, Tokyo 162-0044, Japan
⁵⁶Weizmann Institute, Rehovot 76100, Israel
⁵⁷Yonsei University, IPAP, Seoul 120-749, Korea

(Dated: October 8, 2018)

J/ψ production in $p+p$ collisions at $\sqrt{s} = 200$ GeV has been measured in the PHENIX experiment at the Relativistic Heavy Ion Collider (RHIC) over a rapidity range of $-2.2 < y < 2.2$ and a transverse momentum range of $0 < p_T < 9$ GeV/ c . The statistics available allow a detailed measurement of both the p_T and rapidity distributions and are sufficient to constrain production models. The total cross section times branching ratio determined for J/ψ production is $B_{ll} \cdot \sigma_{pp}^{J/\psi} = 178 \pm 3^{\text{stat}} \pm 53^{\text{sys}} \pm 18^{\text{norm}}$ nb.

PACS numbers: PACS numbers:

J/ψ are produced in hadronic collisions involving hard processes that proceed primarily through diagrams involving gluons, such as gluon-gluon fusion. Once the $c\bar{c}$ pair is produced it must evolve through a hadronization process to form a physical J/ψ . While this production has been extensively studied, the details of the production mechanism and hadronization remain an open question. Attempts at a consistent theoretical description of J/ψ production have been made, but it has proven difficult to reproduce both the observed cross sections and polarization [1, 2, 3, 4]. An additional complication is that nearly 30-40% of the measured J/ψ yield results from feeddown of higher mass states (ψ' , χ_c) [5], reducing the observed polarization with respect to that expected from directly produced J/ψ .

The color-singlet model [6], which generates a color singlet $c\bar{c}$ pair in the same quantum state as the J/ψ , underpredicts the measured J/ψ cross section by approximately an order of magnitude [2]. Alternatively, the color-octet model includes color octet $c\bar{c}$ pairs that radiate soft gluons during J/ψ formation [7]. However, the color octet matrix elements are not universal [8] and the predicted transverse J/ψ polarization at high p_T is not seen in the data [2, 4]. The color evaporation model, a more phenomenological approach, forms the different charmonium states in proportions determined from experimental data for any $c\bar{c}$ pair that has a mass below the $D\bar{D}$ threshold and predicts no polarization. Finally, a recent perturbative QCD calculation including 3-gluon diagrams is able to successfully reproduce both the observed cross section and polarization results [9].

A fundamental understanding of the J/ψ production process is also critical to defining the configuration of the produced $c\bar{c}$ state since this will have direct implications on the interaction of this state with both cold nuclear matter in proton or deuteron-nucleus collisions and with the high-density partonic matter observed in high-energy heavy-ion collisions. High quality experimental results over wide kinematical and collision energy ranges are required to constrain models and to provide an improved understanding of J/ψ (and other heavy quarkonia) production.

In this paper, J/ψ production in $p+p$ collisions at $\sqrt{s} = 200$ GeV measured by the PHENIX experiment at RHIC is reported. The J/ψ cross section and transverse momentum distributions are studied in the mid ($|y| \leq 0.35$) and forward ($1.2 < |y| < 2.2$) rapidity re-

gions. The data presented were collected during the 2005 RHIC run and exceed by more than one order of magnitude the previously reported number of J/ψ [10, 11].

A detailed description of the PHENIX experiment is provided in [12]. At mid-rapidity the drift chambers (DC), ring imaging Čerenkov detectors (RICH), and electromagnetic calorimeters (EMCal) are used to detect $J/\psi \rightarrow e^+e^-$ decays in two arms each covering $\Delta\phi = 90^\circ$ in azimuth. The muon detectors, consisting of cathode strip tracking chambers in a magnetic field (MuTr) and alternating layers of steel absorber and Iarocci tube planes (MuID), are used to measure $J/\psi \rightarrow \mu^+\mu^-$ at forward and backward rapidities over $\Delta\phi = 360^\circ$.

The data were recorded using a minimum bias trigger that requires at least one hit in each of the beam-beam counters (BBC) at forward and backward rapidity, $3.0 < |\eta| < 3.9$. Di-electron events must pass an additional trigger that consisted of an OR between the level-1 electron and photon triggers. The electron trigger requires matching hits between the EMCal and RICH in a small angular area with a minimum energy deposition of 0.4 GeV in any 2×2 patch of EMCal towers. The photon trigger requires a minimum energy deposition of 1.4 GeV in any 4×4 set of overlapping EMCal towers. A J/ψ trigger efficiency of 96% was achieved within the vertex range $|z_{vtx}| < 30$ cm. Di-muon triggered events were selected using an online level-1 trigger that requires at least two particles penetrate the MuID. One particle must penetrate the entire MuID while the second has a minimum penetration depth of 3 out of the 5 pairs of detector and absorber planes. Approximately 92% of the J/ψ 's within $|z_{vtx}| < 30$ cm fulfill this requirement. As part of the reconstruction chain a level-2 filter, which consists of a fast reconstruction of the particle trajectory in the MuTr and MuID is applied. Events are accepted by this filter when at least two particles penetrate the entire MuID and have a reconstructed invariant mass ≥ 2.0 GeV/ c^2 . After applying cuts on the collision vertex position and quality assurance criteria, the sampled statistics corresponds to 2.6 pb^{-1} in the dielectron analysis, 2.7 pb^{-1} in the muon arm covering $1.2 < y < 2.2$ and 3.5 pb^{-1} in the muon arm covering $-2.2 < y < -1.2$.

At mid-rapidity electron candidates are charged tracks associated with at least two hit phototubes in the RICH and one EMCal hit with a position matching of ± 4 standard deviations (σ). The energy-momentum matching requirement is $(E/p - 1)/\sigma \geq -4.0\sigma$. The number of J/ψ

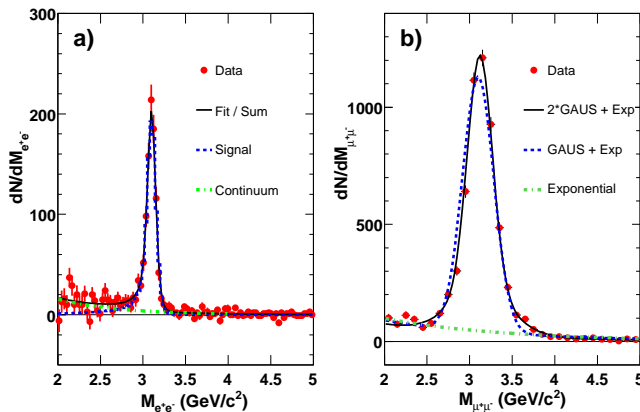


FIG. 1: Invariant mass spectra for a) $J/\psi \rightarrow e^+e^-$ at $|y| < 0.35$ and b) $J/\psi \rightarrow \mu^+\mu^-$ at $1.2 < |y| < 2.2$ with the functional forms used to extract the number of reconstructed J/ψ .

is obtained by counting the unlike-sign dielectron pairs in a fixed mass window after subtracting the like-sign pairs. Figure 1(a) shows the invariant mass spectrum for dielectron pairs after subtracting the like-sign background. The mass window for counting the J/ψ signal is 2.7 - 3.5 GeV/c^2 or 2.6 - 3.6 GeV/c^2 depending on the number of the DC hits used to reconstruct the track. The J/ψ counts are corrected for the continuum yield, which originates primarily from open charm pairs and Drell-Yan, inside the mass window ($10\% \pm 5\%$) and the fraction of J/ψ outside of the mass window ($7.2\% \pm 1.0\%$). Approximately 1500 $J/\psi \rightarrow e^+e^-$ are obtained. The solid line in the figure is the sum of the J/ψ line shape (dashed curve) and an exponential function (dot-dashed curve) describing the continuum component. The J/ψ line shape function includes the detector resolution, the internal radiative effect [13], and the external radiative effect evaluated using a GEANT [14] simulation of PHENIX detector.

Muon track candidates are selected based upon their penetration depth in the MuID and the reconstructed track quality within the MuID and MuTr. The particle trajectory must contain at least 8 of 10 possible hits in the MuID and the position matching between the MuID and MuTr must be within 15(20) cm at positive (negative) rapidity. The J/ψ yield is obtained from the unlike sign dimuon invariant mass distribution by subtracting the combinatorial background estimated using an event mixing technique. Three functions, shown in Fig. 1(b), are used to extract the J/ψ yield. Single Gaussian + exponential and double Gaussian + exponential functions are used to fit the J/ψ peak, while the contribution from the physical continuum and background is estimated using an exponential fit. The reported number of J/ψ represents the average of the fit values. A total of 8000 $J/\psi \rightarrow \mu^+\mu^-$ are obtained. The systematic error associated with the signal extraction is estimated from the

variation between the fits.

The J/ψ cross section in a given rapidity and transverse momentum bin is calculated according to,

$$\frac{B_{ll}}{2\pi p_T} \frac{d^2\sigma_{J/\psi}}{dy dp_T} = \frac{1}{2\pi p_T \Delta p_T \Delta y} \frac{N_{J/\psi}}{\mathcal{L} A \epsilon_{\text{rec}} \epsilon_{\text{trig}} \epsilon_{J/\psi}^{\text{BBC}}},$$

where B_{ll} is the J/ψ dilepton branching ratio, $N_{J/\psi}$ is the measured J/ψ yield, \mathcal{L} is the integrated luminosity recorded by the minimum bias trigger, A ϵ_{rec} represents the geometrical acceptance and reconstruction efficiency, and ϵ_{trig} is the trigger efficiency. $\epsilon_{J/\psi}^{\text{BBC}}$ is the minimum bias trigger efficiency for events containing a J/ψ and was determined to be 0.79 ± 0.02 [10]. The cross section sampled by the BBC trigger, $\sigma_{\text{tot}}^{pp} \times \epsilon_{\text{MB}}^{\text{BBC}} = 23.0 \pm 2.2$ mb, was used to determine the integrated luminosity.

The $A\epsilon_{\text{rec}}$ and ϵ_{trig} terms are determined individually for the central arm and each muon arm based upon the detection of simulated J/ψ processed using the real data analysis chain. Decay events are generated and propagated through a full GEANT simulation of the detector, which includes the specific details of the detector performance including the MuTr and MuID alignment, disabled anodes and MuID efficiency. For the dielectron analysis, corrections to account for the detector dead channel map, energy calibration and run-to-run variations in the detector active area were determined from single electron yields. The J/ψ trigger efficiency is incorporated via a level-1 trigger emulator tuned to describe the experimental trigger response. For the dimuon analysis, the level-2 filtering algorithms are applied to the simulated events. After reconstruction, the number of detected J/ψ is compared to the number of simulated J/ψ in a given rapidity and transverse momentum bin to determine the appropriate correction factors.

The systematic error associated with the measurement of the J/ψ cross section can be divided into three categories based upon the effect each error has on the measured results. All errors are reported as standard deviations. Point-to-point uncorrelated errors, such as the signal extraction systematic, which is bin dependent with typical values of 4% (5%) in the dimuon (dielectron) data, allow the data points to move independently with respect to one another. Point-to-point correlated errors allow the data points to move coherently within the quoted value. Their values amount to 10% (8%) for the detector acceptance, 8% (4%) for the run-to-run variation in the detector efficiency, 4% (2.5%) for the J/ψ transverse momentum and vertex distributions, and 2% (2%) for the hardware efficiency of the detector. Finally, global systematic errors allow the data points to move together. The dominant source of this error originates from the estimation of the BBC triggering efficiency for minimum bias events, 9.7%, with additional contribution from the uncertainty in the estimation of the number of sampled minimum bias events, 1%, and $\epsilon_{J/\psi}^{\text{BBC}}$, 2.5%.

Figure 2(a) shows the transverse momentum spectra at both mid and forward rapidities, which are fit with the function, $A \times (1 + (p_T/B)^2)^{-6}$ [15], to extract the $\langle p_T^2 \rangle$. At mid-rapidity $\langle p_T^2 \rangle = 4.14 \pm 0.18 \pm_{0.20}^{0.30}$ (GeV/c)² and the χ^2 per degree of freedom (χ^2/ndf) is 23/19. At forward rapidity $\langle p_T^2 \rangle = 3.59 \pm 0.06 \pm 0.16$ (GeV/c)² and the χ^2/ndf is 28/17. The first error is statistical and the second includes the systematic error from the maximum shape deviation permitted by the point-to-point correlated errors and from allowing the exponent of the fit function to be a free parameter. Although good agreement is found with the rapidity distribution and total cross section, previously published results [11] yielded a significantly lower $\langle p_T^2 \rangle$ at forward rapidity than found here, even accounting for the quoted statistical and systematic uncertainties. The increased statistics of the present data set allow for an improved understanding of the shape of the p_T spectrum at forward rapidity due to the extended range in p_T and the finer binning at low p_T . The previous results have been revisited and it was found that the systematic error was underestimated.

Figure 2(b) shows the ratio of the invariant cross section at forward and mid-rapidity. The ratio falls with p_T and reaches a minimum of 0.5 above a p_T of 2 GeV/c. The data indicates that the forward rapidity p_T distribution is substantially softer than mid-rapidity. This is attributed to the increase in the longitudinal momentum at forward rapidity leaving less energy available in the transverse direction.

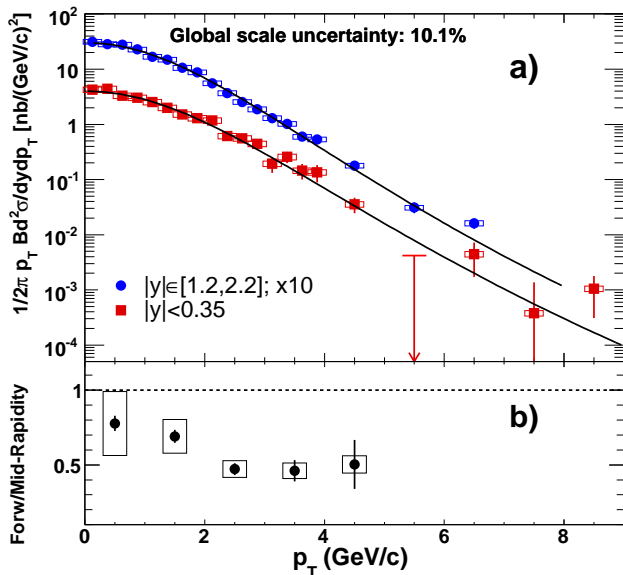


FIG. 2: (a) The mid and forward rapidity J/ψ differential cross section times dilepton branching ratio versus p_T and (b) the ratio of the mid and forward p_T spectra. The vertical error bars are the statistical and point-to-point uncorrelated error and the boxes are the point-to-point correlated systematic error. The solid lines are the fits described in the text.

The observed p_T distributions are substantially harder

than those for lower energy $p+p$ and $p+A$ collisions as expected from the increased phase space at higher energy. Figure 3 shows the energy dependence of the average $\langle p_T^2 \rangle$ including lower energy points from the Super Proton Synchrotron, and Fermilab fixed target and Tevatron measurements. A linear fit versus the log of the center of mass energy describes the general trends, although some variation is expected due to the differing rapidity ranges of the measurements and the use of $p+A$ data for some of the points.

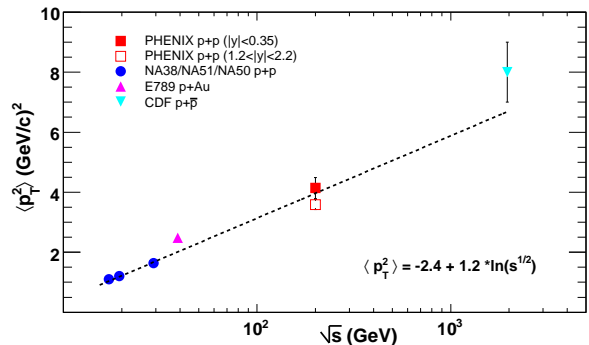


FIG. 3: PHENIX $\langle p_T^2 \rangle$ measurements compared to measurements at other energies [4, 16, 17] as a function of collision energy for J/ψ production in $p+p$ or $p+A$ collisions. Also shown is a linear fit vs $\ln(\sqrt{s})$.

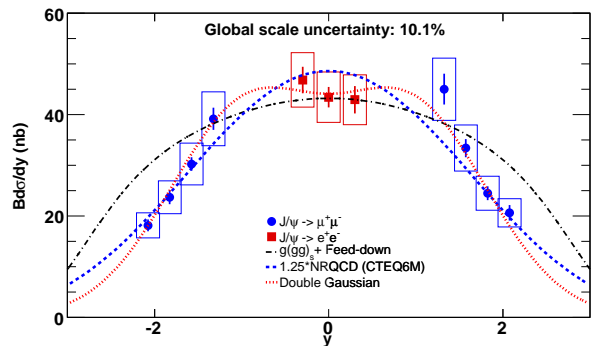


FIG. 4: The J/ψ differential cross section times dilepton branching ratio plotted versus rapidity. The vertical error bars represent the statistical and point-to-point uncorrelated error and the boxes represent the point-to-point correlated systematic error. The curves are described in the text.

Figure 4 shows the J/ψ differential cross section vs rapidity. The statistics of these results are large enough to allow eleven rapidity bins to be measured compared to the five bins used in the previous measurement [11]. Also shown are several model fits to the data. The dashed curve is a non-relativistic QCD calculation [18]. The dot-dash curve is a pQCD calculation that includes diagrams describing a third gluon, which is necessary to neutralize the otherwise colored states [9]. This model fails to reproduce the steeply falling cross section observed in

the present data at large rapidity. An empirical double Gaussian fit (dot-dot curve) is able to reproduce the data best, but has no strong theoretical foundation. The data slightly favor a flatter distribution over the rapidity range $|y| < 1.5$ than most models, but since the systematic error on the mid and forward rapidity points are independent, a narrower distribution is not excluded.

To determine the total cross section, the rapidity distribution was fit with many theoretical and phenomenological shapes, including those shown in Fig. 4. We obtain a total cross section times branching ratio of $B_{ll} \cdot \sigma_{pp}^{J/\psi} = 178 \pm 3^{\text{stat}} \pm 53^{\text{sys}} \pm 18^{\text{norm}}$ nb. The absolute normalization error (norm) represents the uncertainty in the BBC trigger cross section. The systematic error (sys) is estimated from the maximum variation allowed by shifting the mid and forward rapidity data independently by their point-to-point correlated systematic errors. This result is consistent with our previous measurement [11].

We have presented J/ψ results for $p+p$ collisions at $\sqrt{s} = 200$ GeV that extend the reach in transverse momentum to 9 GeV/ c . The measured p_T spectrum is harder than that observed at lower energies and also shows a softening at forward rapidity. The rapidity shape falls steeply at forward rapidity and can not be reproduced by the pQCD calculation in [9]. Furthermore, the data slightly favor a flatter rapidity distribution than most models, but a narrower distribution is not excluded. These data not only constrain production models for heavy quarkonia, but also provide a critical baseline for similar studies in deuteron-nucleus and heavy-ion collisions [19, 20].

We thank the staff of the Collider-Accelerator and Physics Departments at BNL for their vital contributions. We acknowledge support from the Department of Energy and NSF (U.S.A.), MEXT and JSPS (Japan), CNPq and FAPESP (Brazil), NSFC (China), MSMT (Czech Republic), IN2P3/CNRS, and CEA (France), BMBF, DAAD, and AvH (Germany), OTKA (Hungary), DAE (India), ISF (Israel), KRF and KOSEF (Korea), MES, RAS, and FAEF (Russia), VR and KAW (Sweden), U.S. CRDF for the FSU, US-Hungarian NSF-

OTKA-MTA, and US-Israel BSF.

* Deceased

† PHENIX Spokesperson: zajc@nevis.columbia.edu

- [1] M. Beneke, M. Kraemer, Phys. Rev. **D55**, 5269 (1997); M. Beneke, I. Z. Rothstein, Phys. Rev. **D54**, 2005 (1996).
- [2] F. Abe *et al.*, Phys. Rev. Lett. **69**, 3704 (1992); F. Abe *et al.*, Phys. Rev. **D66**, 092001 (2002); S. Abachi *et al.*, Phys. Lett. **B370**, 239 (1996); B. Abbot *et al.*, Phys. Rev. Lett. **82**, 35 (1999).
- [3] R. Vogt, Phys. Repts. **310**, 197 (1999).
- [4] M. H. Schub *et al.*, Phys. Rev. **D52**, 1307 (1995).
- [5] I. Abt *et al.*, Phys. Lett. **B561**, 61 (2003).
- [6] E. L. Berger *et al.*, Phys. Rev. **D23**, 1521 (1981); R. Baier *et al.*, Phys. Lett. **B102**, 364 (1981).
- [7] G. T. Bodwin *et al.*, Phys. Rev. **D51**, 1125 (1995); erratum Phys. Rev. **D55**, 5853 (1997).
- [8] J. K. Mizukoshi, SLAC-PUB-8296, hep-ph/9911384 (1999).
- [9] V. A. Khoze *et al.*, Eur. Phys. J. **C39**, 163-171 (2005) and private communications.
- [10] S. S. Adler *et al.*, Phys. Rev. Lett. **92**, 051802 (2004).
- [11] S. S. Adler *et al.*, Phys. Rev. Lett. **96**, 012304 (2006).
- [12] K. Adcox *et al.*, Nucl. Instr. Meth. **A499**, 469 (2003).
- [13] A. Spiridonov, hep-ex/0510076 (2004).
- [14] GEANT 3.2.1, CERN Computing Library, <http://wwwasd.web.cern.ch/wwwasd/geant/index.html>.
- [15] J. K. Yoh *et al.*, Phys. Rev. Lett. **41**, 684 (1978); and private communication..
- [16] O. Drapier, Thèse d'habilitation, Université Claude Bernard - Lyon 1, 1998; available at <http://na50.web.cern.ch/NA50/theses.html>.
- [17] D. Acosta *et al.*, Phys. Rev. **D71**, 032001 (2005). The $\langle p_T^2 \rangle$ was extracted using a fit of the form $A \times (1 + (p_T/B)^2)^{-6}$.
- [18] F. Cooper *et al.*, Phys. Rev. Lett. **93**, 171801 (2004); and private communication.
- [19] S. S. Adler *et al.*, (Au+Au J/ψ paper, preprint number soon).
- [20] S. S. Adler *et al.*, (Cu+Cu J/ψ paper, preprint number soon).